

Post-mitotic dynamics of pre-nucleolar bodies is driven by pre-rRNA processing

Coralie Carron^{1,2}, Stéphanie Balor^{3,4}, Franck Delavoie^{1,2}, Célia Plisson-Chastang^{1,2}, Marlène Faubladier^{1,2}, Pierre-Emmanuel Gleizes^{1,2,*} and Marie-Françoise O'Donohue^{1,2}

¹Université de Toulouse, UPS, Laboratoire de Biologie Moléculaire Eucaryote, F-31000 Toulouse, France

²CNRS, UMR 5099, F-31000 Toulouse, France

³CNRS, Fédération de Recherche en Biologie de Toulouse, F-31000 Toulouse, France

⁴Université de Toulouse, UPS, FR 3451, F-31000 Toulouse, France

*Author for correspondence (gleizes@ibcg.bioto.toul.fr)

Accepted 7 June 2012

Journal of Cell Science 125, 4532–4542

© 2012. Published by The Company of Biologists Ltd

doi: 10.1242/jcs.106419

Summary

Understanding the relationship between the topological dynamics of nuclear subdomains and their molecular function is a central issue in nucleus biology. Pre-nucleolar bodies (PNBs) are transient nuclear subdomains, which form at telophase and contain nucleolar proteins, snoRNPs and pre-ribosomal RNAs (pre-rRNAs). These structures gradually disappear in early G1 phase and are currently regarded as reservoirs of nucleolar factors that participate to post-mitotic reassembly of the nucleolus. Here, we provide evidence from fluorescence *in situ* hybridization and loss-of-function experiments in HeLa cells that PNBs are in fact active ribosome factories in which maturation of the pre-rRNAs transiting through mitosis resumes at telophase. We show that the pre-rRNA spacers are sequentially removed in PNBs when cells enter G1 phase, indicating regular pre-rRNA processing as in the nucleolus. Accordingly, blocking pre-rRNA maturation induces accumulation in PNBs of stalled pre-ribosomes characterised by specific pre-rRNAs and pre-ribosomal factors. The presence of pre-ribosomal particles in PNBs is corroborated by observation of these domains by correlative electron tomography. Most importantly, blocking pre-rRNA maturation also prevents the gradual disappearance of PNBs, which persist for several hours in the nucleoplasm. In a revised model, we propose that PNBs are autonomous extra-nucleolar ribosome maturation sites, whose orderly disassembly in G1 phase is driven by the maturation and release of their pre-ribosome content.

Key words: Ribosome biogenesis, *Homo sapiens*, Pre-ribosomal RNA processing, Pre-nucleolar bodies, Mitosis

Introduction

During open mitosis, the nucleolus is disassembled like all nuclear domains. Both ribosomal DNA (rDNA) transcription and processing of pre-ribosomal particles are progressively switched off during prophase and then reactivated in telophase (Gébrane-Younès et al., 1997). In prophase, rDNA transcription by RNA polymerase I is inhibited through successive phosphorylation of its co-factors by the cyclin-dependent kinase 1 (CDK1)/cyclinB complex (Heix et al., 1998; Sirri et al., 1999). Numerous components of the transcription machinery, including UBF and most RNA polymerase I subunits, remain associated with the rDNA genes in an inactive form, whereas other proteins transiently dissociate from the transcriptional complexes and relocate to the cytosol (Chen et al., 2005; Leung et al., 2004; Roussel et al., 1996; Sirri et al., 1999; Zatsepina et al., 1993). Although the pre-rRNA processing machinery is inhibited during mitosis, stable pre-rRNAs are detected in mitotic cells (Beven et al., 1996; Dousset et al., 2000; Dundr and Olson, 1998; Dundr et al., 2000; Fan and Penman, 1971; Piñol-Roma, 1999). When transcription is shut down, these pre-rRNAs progressively diffuse from the nucleoli to the cytosol and form a sheath around the condensed chromosomes in metaphase; they are also detected in a few cytosolic foci called nucleolar-derived foci (NDF), which persist in the cytosol of daughter cells until early G1 (Dundr and Olson, 1998; Dundr et al., 2000). In telophase, the transcriptional machinery is reactivated at

the nucleolar organiser regions (i.e. the active rDNA loci), where nucleoli reform. As the chromosomes start to unwind, the perichromosomal sheath breaks down into pre-nucleolar bodies (PNBs), which contain pre-rRNAs, but not the RNA polymerase I machinery (Chan et al., 1991; Dundr and Olson, 1998; Dundr et al., 2000; Fomproix and Hernandez-Verdun, 1999; Jimenez-Garcia et al., 1994; Roussel et al., 1993; Savino et al., 1999). Some PNBs fuse with the reforming nucleoli at telophase/early G1, while others remain in the nucleoplasm and progressively resorb in G1.

Based on their content and on their morphology, PNBs have long been considered as intermediates in the reconstitution of the incipient nucleoli. More recently, it has been proposed that pre-rRNAs present in PNBs might act as assembly sites, complexing processing factors before their incorporation into the nucleolus (Angelier et al., 2005; Dousset et al., 2000; Dundr et al., 2000; Muro et al., 2010; Savino et al., 2001). According to this hypothesis, the stability of the pre-rRNAs is the key factor that governs retention of nucleolar proteins in PNBs. However, the underlying determinants of pre-rRNA stability have remained vague. In addition, direct evidence in support of a role of PNBs in nucleolus re-assembly is still lacking.

In eukaryotes, rDNA transcription in the nucleolus produces a large polycistronic precursor, called 47S pre-rRNA in vertebrates. This early pre-rRNA contains the sequences of the 18S, 5.8S and 28S rRNAs, flanked by external and internal transcribed spacers

(ETSs and ITSs; Fig. 1). A subset of ribosomal proteins and pre-ribosomal factors assemble co-transcriptionally with the 47S pre-rRNA, forming the 90S pre-ribosomal particle (Henras et al., 2008; Pérez-Fernández et al., 2007). Pre-ribosomal particles are then further matured by the sequential removal of the ETS and ITS sequences, through endonucleolytic cleavages or exonucleolytic processing (Borovjagin and Gerbi, 2005; Eichler and Craig, 1994; Hadjiolov, 1985). Cleavage of the ITS1 at site 2 (Fig. 1) splits the 90S particle into pre-40S and pre-60S ribosomal particles, which then follow distinct maturation pathways. The final processing steps take place after export into the cytoplasm, leading to the two mature ribosomal subunits (Rouquette et al., 2005; Thomson and Tollervey, 2010). Pre-rRNA maturation involves almost 200 *trans*-acting proteins and over 100 small nucleolar RNPs (snoRNPs) that intervene sequentially in an intricate ballet of assembly and disassembly steps, as shown in the yeast *Saccharomyces cerevisiae* (Fatica and Tollervey, 2002; Henras et al., 2008; Kressler et al., 2010).

Current knowledge regarding the fate of the pre-rRNAs in PNBs is fragmentary. Fluorescence *in situ* hybridization (FISH) experiments have shown that PNBs contain partially processed pre-rRNAs lacking the 5'-ETS leader sequence and the 3'-ETS (Dundr and Olson, 1998; Dundr et al., 2000), two sequences that are removed early in the processing pathway. In addition, the 5'-ETS was detected in PNBs at telophase, but not in G1 phase. A number of *trans*-acting factors have been localised in PNBs, together with pre-rRNAs, including the small nucleolar RNAs (snoRNAs) U3 and U14 and some pre-ribosomal proteins (for a review, see DiMario, 2004). Strikingly, these factors exit from the PNBs in an ordered way that correlates with the order in which they participate in pre-rRNA processing. Proteins required for the earliest steps of ribosome biogenesis, such as fibrillarin, leave PNBs first, while pre-ribosomal factors (e.g. Bop1, Nop52 or B23), which participate in subsequent steps, reside in PNBs for a longer period of time (Angelier et al., 2005; Dundr et al., 2000;

Leung et al., 2004; Savino et al., 1999; Savino et al., 2001). Pre-ribosomal factors in PNBs are rapidly exchanged with the rest of the nucleus and can establish functional interactions in PNBs, as shown for Nop52 and B23 (Muro et al., 2010).

Here we have investigated whether pre-rRNAs are subjected to maturation in PNBs, like pre-rRNAs in the nucleolus. Consistent with this idea, PNBs were previously shown to contain PM-Scl100, a component of the exosome, a multi-enzymatic exonucleolytic complex involved in pre-rRNA processing (Fomproix and Hernandez-Verdun, 1999). We have found that this hypothesis is fully supported by the evolution of pre-rRNAs in PNBs from mitosis to G1, by loss-of-function experiments targeting pre-rRNA processing, as well as by the observation of the subcellular structure of PNBs by electron tomography. These results offer a parsimonious explanation for the ordered release of pre-ribosomal factors from PNBs as pre-ribosome maturation progresses. In the light of these data, we argue that PNBs are primarily maturation sites for mitotic pre-rRNAs.

Results

Pre-rRNAs in PNBs evolve from early to late precursors

To determine whether pre-rRNAs were processed in PNBs, we looked at their evolution from mitosis to G1. FISH was carried out with a combination of seven probes complementary to different segments of the transcribed spacers to discriminate early versus late precursors (Fig. 1). This experiment was performed on asynchronous HeLa cells expressing B23/nucleophosmin fused to GFP (HeLa GFP-B23), a well-described marker of PNBs (Louvet et al., 2005). Labelling by the different probes of NDFs and PNBs, detected with GFP-B23, was scored in cells from anaphase to G1 phase (Fig. 2).

In mitotic cells, from prometaphase to telophase, probes complementary to the 5'-ETS, ITS1 or ITS2 labelled both the chromosomal sheath and the NDFs (Fig. 2A,B). No labelling was observed in these structures with probes specific either for the 5'-

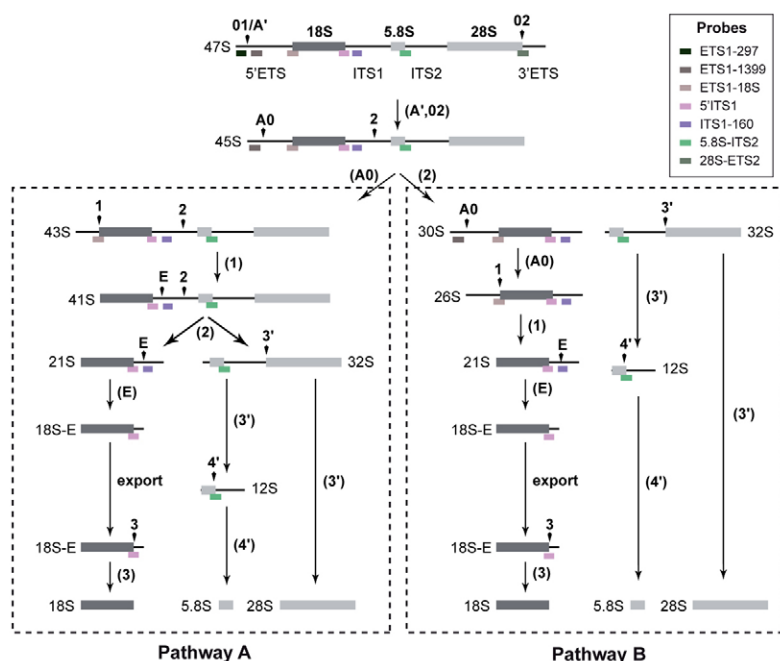


Fig. 1. Pre-rRNA processing pathways in human cells.

Maturation proceeds through multiple cleavages (represented by arrowheads). They affect either the external transcribed spacers (5'-ETS and 3'-ETS) flanking the 18S and 28S rRNAs, or the internal transcribed spacers (ITS1 and ITS2). Pathway B is predominant in HeLa cells. The probes used to detect the pre-rRNAs in FISH experiments are drawn as coloured boxes.

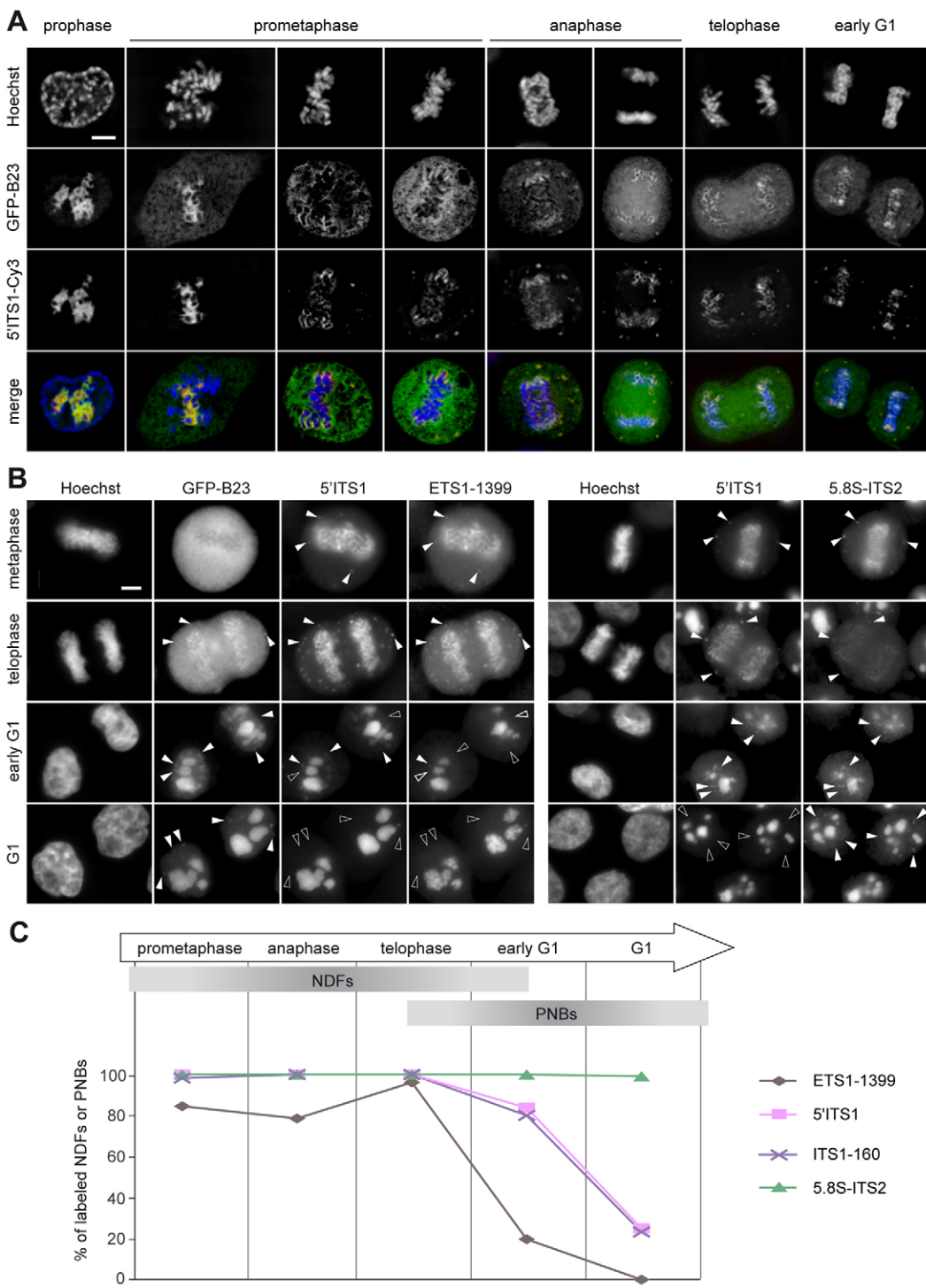


Fig. 2. Evolution of the pre-rRNA content of PNBs through mitosis and G1 phase. The nature of the pre-rRNAs contained in NDFs and PNBs was assessed in HeLa GFP-B23 cells during mitosis and early G1 by dual-probe FISH experiments. (A) Single planes were selected out of deconvoluted stacks representative of the different steps of mitosis. B23 and the precursors to the 18S rRNA, revealed by the 5'ITS1 probe, colocalised in the perichromosomal sheath, NDFs and PNBs. Similar results were obtained with the ETS1-1399 and 5.8S-ITS2 probes. (B) Single plane images were acquired of mitotic or G1 cells bearing NDFs and/or PNBs. Arrowheads point to representative PNBs: filled arrowheads indicate labelling of the PNB with the corresponding probe, and absence of labelling is indicated by open arrowheads. The gamma value was set to 1.4. (C) PNBs and NDFs detected with GFP-B23 and scored for the presence of each probe. A minimum of 13 mitotic cells, 14–19 cells in early G1 and 10–19 cells in G1 were studied for each experimental condition. Scale bars: 5 μm.

ETS leader sequence (ETS1-297) or for the 3'-ETS (probe 28S-3'ETS), indicating that mitotic pre-rRNAs had already undergone the earliest cleavages at site A' and at the end of the 28S segment (data not shown). Cells in late anaphase/telophase displayed NDFs and PNBs labelled with GFP-B23. At this stage, these structures were all labelled with the 5'-ETS-, ITS1- and ITS2-specific probes (Fig. 2B,C). In contrast, only 20% of the PNBs contained 5'-ETS in early G1 cells, indicating the loss of early rRNA precursors. Furthermore, while the ITS2-specific probes labelled all the PNBs, the ITS1 was only detected in 80% of them (Fig. 2B,C). In cells further engaged in G1, displaying smaller and fewer PNBs in rounder and larger nuclei, PNBs were only labelled with ITS2-specific probes, indicating the sole presence of 60S subunit precursors (Fig. 2B,C). We never detected PNBs containing ITS1 without ITS2, or 5'-ETS without ITS1 and ITS2, indicating that the presence of pre-rRNAs in PNBs is not random, but rather follows a precise timing (Fig. 2C): the 5'-ETS is first to disappear at the end of telophase, followed by the ITS1 in early

G1 and ultimately by the ITS2, which corresponds exactly to elimination of the transcribed spacers during pre-rRNA processing. Importantly, PNBs remained negative upon staining of the cells for 30 minutes by ethynyl-uridine (EU), indicating that no neosynthesised pre-rRNAs transited through these structures (supplementary material Fig. S1).

Specific pre-rRNAs accumulate in PNBs upon ribosomal protein knockdown

These observations were fully consistent with pre-rRNA maturation taking place in PNBs. To further challenge this hypothesis on mechanistic grounds, we checked whether altering pre-rRNA processing could specifically modulate the fate of pre-rRNAs in PNBs. We knocked down a series of ribosomal proteins involved in the biogenesis of the small or the large subunits, from early to late stages. Upon knockdown of the small ribosomal subunit protein RPS29, which affects the maturation of the 21S and 18S-E pre-rRNAs (O'Donohue et al., 2010), PNBs in cells exiting

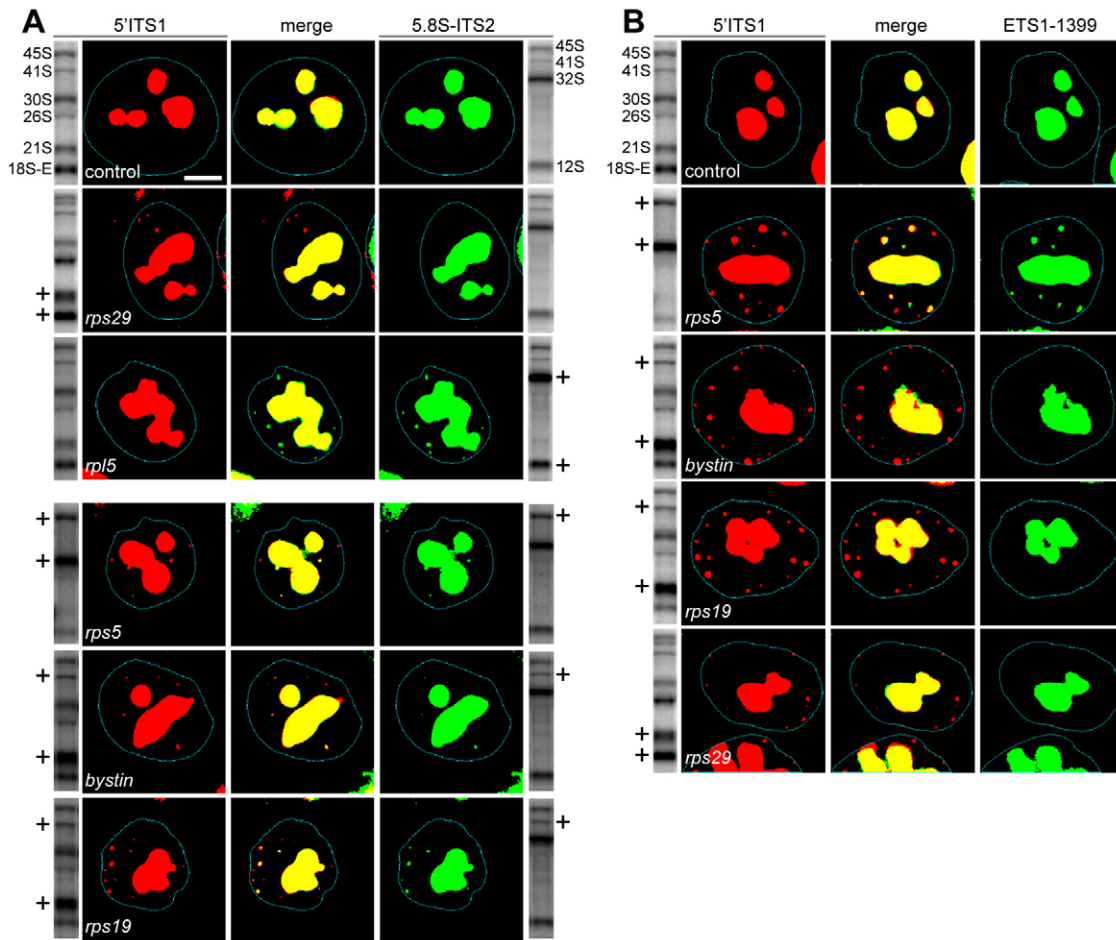


Fig. 3. Specific pre-rRNA species accumulate within PNBs after knockdown of ribosomal proteins. HeLa cells, subjected for 48 h to siRNA treatment, were hybridised with combinations of two probes labelled either with Cy3 or Cy5 (see position of the probes in Fig. 1). Northern blots on the sides show the pre-rRNA species accumulating upon protein depletion (+). All images were captured under identical conditions. Because the fluorescence intensity of PNBs was low compared to that of the nucleoli, images were subjected to a top-hat filter and a median filter, background was subtracted and grey levels were binarised. This procedure provided a clear identification of PNBs and nucleoli without loss of information. The nuclear periphery was delineated by a blue line. (A) Probes 5'ITS1-Cy3 (red) and 5.8S-ITS2-Cy5 (green). (B) Probes 5'ITS1-Cy3 (red) and ETS1-1399-Cy5 (green). Co-localisation in the merged images appears in yellow. Scale bar: 5 μ m.

mitosis contained ITS1 and ITS2 (supplementary material Fig. S2). The 5'-ETS disappeared at telophase, as observed in control cells (data not shown). However, at later stages in G1, we observed the persistence of the ITS1 in PNBs that did not contain ITS2 anymore, consistent with the accumulation of 21S and 18S-E pre-rRNAs observed on northern blot (Fig. 3A). In contrast, depletion of the large ribosomal subunit protein RPL5 caused accumulation of PNBs labelled with the ITS2-specific probe, but not with the ITS1-specific probes (Fig. 3A). When proteins necessary for processing of the 5'-ETS were depleted, like RPS5, RPS6 or RPS24, this transcribed spacer remained visible in PNBs of G1 cells, as illustrated for RPS5 in Fig. 3B; these late PNBs were also labelled both with the ITS1- and the ITS2-specific probes, consistent with accumulation of 30S and 45S pre-rRNAs (Fig. 3A). An intermediate situation was observed when RPS19 was knocked down: late PNBs contained the ITS1 and ITS2 (Fig. 3A), but not the 5'-ETS, as expected from the accumulation of 21S and 41S pre-rRNAs observed in RPS19-depleted cells (Fig. 3B). This observation was not limited to ribosomal proteins since similar results were observed upon knockdown of bystin/ENP1, a pre-ribosomal factor required for the same maturation steps as RPS19 (Fig. 3B).

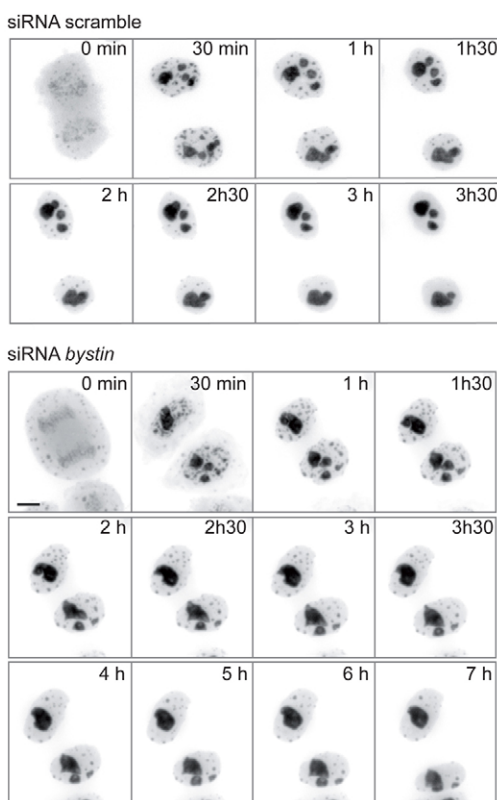


Fig. 4. Disappearance of PNBs in G1 phase is blocked upon pre-rRNA processing knockdown. Time-lapse (3D + time) microscopy was carried out in HeLa GFP-B23 cells 48 h after transfection with a scramble siRNA or with a mixture of siRNAs *bystin-1* and *bystin-2*. Z-stacks were acquired every 30 min with a spinning disk confocal microscope starting at anaphase/early telophase and during progression through G1 phase for up to 7 h. The galleries present a maximal intensity projection of each z-stack with an inverted contrast (see supplementary material Movie 2). Similar results were obtained upon depletion of RPS19 or RPS24. Scale bar: 5 μ m.

Pre-rRNA maturation defects block PNB disappearance in G1 phase

In addition to changing the content in pre-rRNAs of PNBs, perturbing pre-rRNA maturation also resulted in a significant increase of the proportion of interphase cells containing PNBs (30–50%) as compared to control cells (10%), suggesting a difference in the lifetime of PNBs (see Fig. 5). This led us to assess the dynamics of PNBs in cells depleted of RPS19 or bystin by performing time-lapse fluorescence microscopy with GFP-B23, from anaphase to G1. The kinetics of the formation of PNBs at the end of mitosis was similar to control cells: a fraction of them fused with the incipient nucleoli, while the others remained isolated in the nucleoplasm (illustrated for RPS19 depletion in supplementary material Fig. S3; Movie 1). But in contrast to control cells, in which PNBs disappeared within 2–3 hours, a large number of PNBs persisted for several hours in the nucleoplasm of cells depleted of RPS19 or bystin (illustrated for bystin in Fig. 4; supplementary material Movie 2). Therefore, altering pre-rRNA processing not only changed the pre-rRNA composition of late PNBs, but also strongly delayed the progressive dissolution of PNBs in G1. These data indicate that PNB disappearance in G1 depends on the processing of the pre-rRNAs that they contain. By labelling the cells with 5-ethynyl-2'-deoxyuridine (EdU), we verified that the persistent PNBs observed in RPS19-depleted cells were present in G1 phase, but not in S and G2 phase (Fig. 5). As reported before (Miyake et al., 2008), we also observed that depletion of RPS19 induced an arrest or a strong delay of the cells in G1 phase (not shown).

Specific pre-ribosomal particles accumulate in stalled PNBs

The pre-ribosomes accumulating in PNBs upon alteration of pre-rRNA processing were further characterised by detecting some pre-ribosomal factors, either with specific antibodies or by expressing fluorescent fusion proteins. Upon knockdown of RPSs, proteins

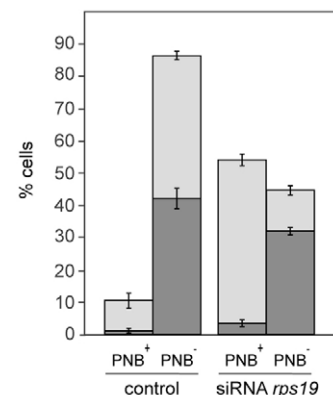


Fig. 5. PNBs accumulate in G1 phase in cells treated with siRNA *rps19*. Multiplex image cytometry was carried out to assess the relationship between residual PNBs and the cell cycle. Two days after transfection with a scramble siRNA or siRNA *rps19*, EdU was added for 4 h to label cells in S and G2 phases. The residual PNBs were detected by FISH with the 5'ITS1 probe and DNA was stained with DAPI. Images of 700–1100 nuclei were collected for each condition. Nuclei were counted and assessed for the presence of EdU labelling and PNBs. The percentage of nuclei in which PNBs are either absent or present is shown. The proportion of EdU-positive nuclei is superimposed in dark grey. Means \pm s.d. of three independent experiments are shown.

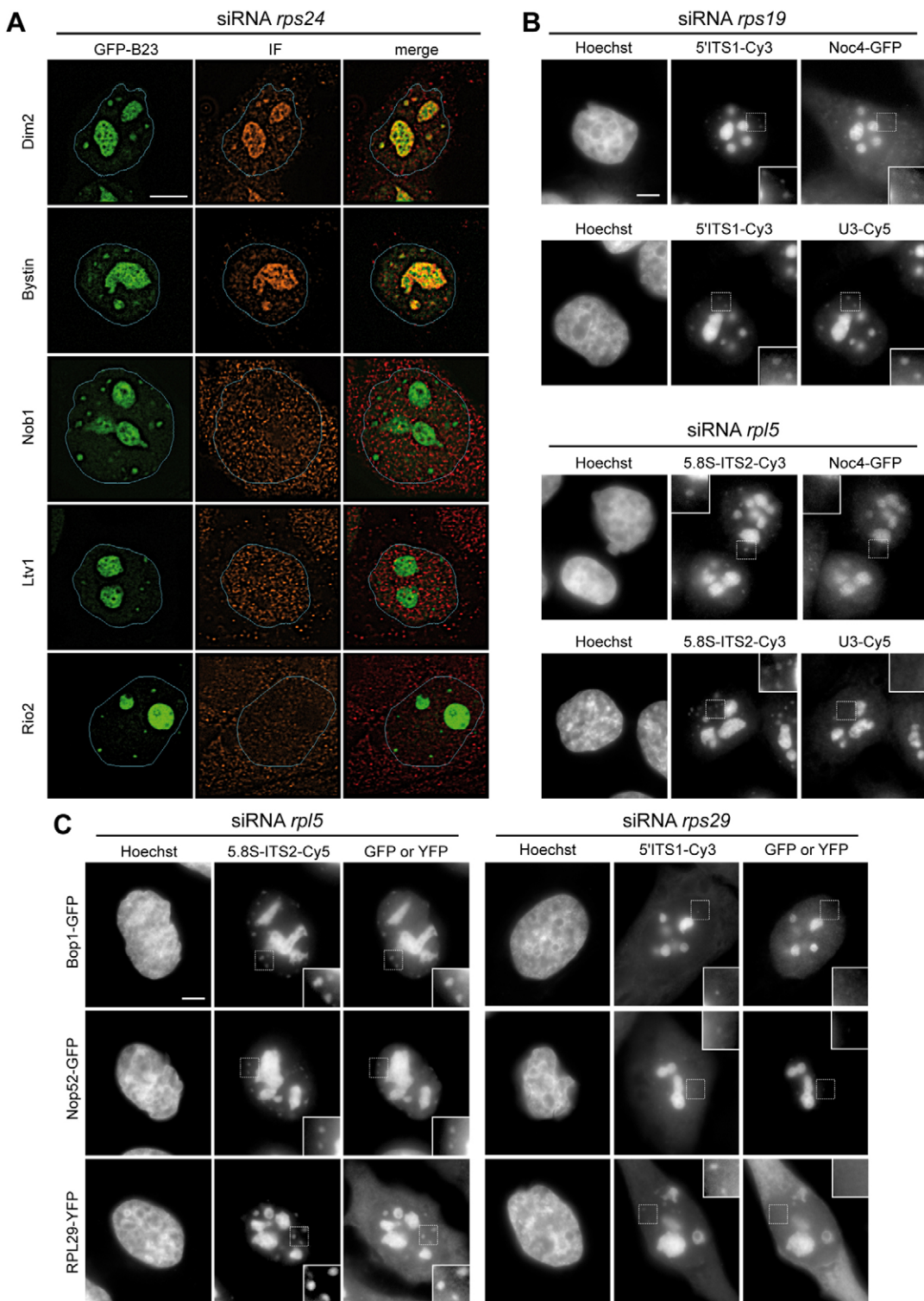


Fig. 6. Stalled PNBs contain specific pre-ribosomal factors and snoRNAs. HeLa GFP-B23, HeLa RPL29-YFP and HeLa cells were treated for 48 h with *rps24*, *rps19*, *rps29* or *rp5* siRNAs and compared to controls. (A) Immunodetection of pre-ribosomal factors that bind to 90S or pre-40S particles in RPS24-depleted cells. Images were deconvoluted with the nearest-neighbour algorithm. Nuclei are delineated in blue. (B) HeLa cells, co-transfected with pNoc4-GFP and *rps19* or *rp5* siRNAs, were analysed by FISH, with either the 5'ITS1 or the 5.8S-ITS2 probes conjugated to Cy3. Alternatively, FISH was performed on HeLa cells treated with the same siRNAs with probes U3-Cy3 and 5'ITS1-Cy5 or 5.8S-ITS2-Cy5. (C) HeLa cells transfected with either pGFP-Bop1 or pEGFP-Nop52, or HeLa RPL29-YFP cells, were analysed by FISH with probes 5'ITS1-Cy3 or 5.8S-ITS2-Cy3. All images are displayed with a gamma set to 1.4. Scale bars: 5 μ m.

hDim2, bystin/hEnp1 and hNoc4, three components of the 90S and pre-40S particles, accumulated in PNBs together with the U3 snoRNA, which is involved in several steps of the small subunit maturation pathway (Borovjagin and Gerbi, 2005) [illustrated in Fig. 6A,B for *rps19* short interfering RNA (siRNA)-treated cells]. In contrast, none of these components was detected in PNBs persisting after depletion of RPL5, as illustrated for hNoc4 and U3 (Fig. 6B). They contained in turn the pre-60S ribosomal factors Bop1 (Lapik et al., 2004) and Nop52 (Savino et al., 1999), as well as the large ribosomal subunit protein RPL29 (Fig. 6C). Neither Bop1, nor Nop52, nor RPL29 were present in PNBs persisting upon knockdown of RPSs or bystin (Fig. 6C; supplementary material Fig. S2 for RPS29 knockdown). NPM/B23 was always observed in persistent PNBs, irrespective of the siRNA used, in agreement with the versatile function of this protein in the production of both ribosomal subunits (Lindström, 2011). The snoRNP protein fibrillarin and the U8 snoRNA, which participate in early maturation steps, were always absent from late PNBs (data not shown).

These results are fully consistent with the presence of partially assembled pre-ribosomal particles in PNBs upon interruption of the maturation process. Interestingly, late PNBs accumulating upon RPSs knockdown contained neither the late pre-40S particle components hLtv1 and hRio2, which are presumably involved in nuclear export and final cytoplasmic processing of the pre-40S particles (Rouquette et al., 2005; Wild et al., 2010; Zemp et al., 2009), nor hNob1, the putative endonuclease ensuring the ultimate cleavage of the 3' end of the 18S rRNA in the cytoplasm (Lamanna and Karbstein, 2009) (Fig. 6A). These late pre-ribosomal factors were not detected in nucleoli either (Fig. 6A), unlike hDim2, bystin and Noc4, which suggests that the presence of pre-ribosomal factors in PNBs obeys the same laws as in nucleoli.

Correlative electron tomography shows pre-ribosomal particles in PNBs

Finally, we sought to directly visualise the pre-ribosomal particles in PNBs by correlative electron tomography in HeLa GFP-B23 cells. GFP-labelled PNBs were first detected in ultrathin sections by fluorescence microscopy before observation by transmission electron microscopy (Fig. 7A). In conventional electron micrographs, PNBs appeared as dense fibrillo-granular bodies, often located in the vicinity of the nuclear envelope (Fig. 7B,C), similar to previous descriptions (Azum-Gélaïde et al., 1994; Dundr et al., 2000; Savino et al., 2001). When these structures were imaged by electron tomography, isolated particles became more clearly distinguishable in PNBs (Fig. 7D) and could be segmented in three dimensions (Fig. 7E,F). For a large fraction of the particles, the size of the bounding boxes (minimal bounding rectangles) framing their median section in the tomogram was in the same range as projections of randomly oriented 40S and 60S ribosomal subunits, arguing for these particles being medium or late pre-ribosomal intermediates (Fig. 7G). In addition, larger complexes (up to 30 nm in length) were observed, potentially corresponding to early pre-ribosomes. Indeed, the size range of the particles in PNBs of RPS19-depleted cells was narrower than in control cells: it matched the computed dimensions of the 40S subunit (Fig. 7G; F-test: $P>0.15$ for both dimensions), consistent with the accumulation of late nuclear pre-40S particles in these structures. These structural data are in good agreement with the molecular characterisation of PNBs presented above. Taken together, these

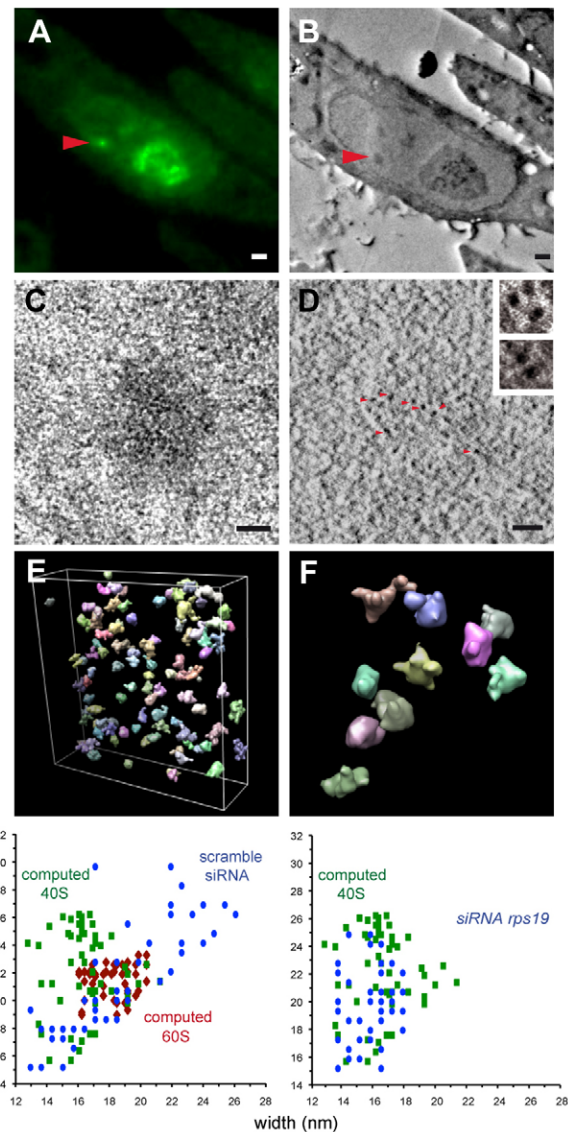


Fig. 7. Visualisation of pre-ribosomal particles in PNBs by correlative electron tomography in HeLa GFP-B23. (A-D) PNBs (arrows in A and B) were first identified in ultrathin sections by fluorescence microscopy (A), and then observed by transmission electron microscopy (B; enlarged in C) and electron tomography (D). In the sections of the reconstructed tomograms (D), isolated particles are clearly detected (insets). (E,F) Visualisation of the isolated particles by volume rendering after 3D segmentation. The example shown in A-F is typical of cells treated with *rps24* siRNA. (G) The dimensions of the bounding boxes of the particles observed in PNBs of control cells or RPS19-depleted cells were plotted as width versus length and compared to those of the 40S (green) and 60S (red) particles projected along multiple orientations (see Materials and Methods). Scale bars: 250 nm in A and B, 100 nm in C and D.

results strongly support that mitotic pre-rRNAs gathering in PNBs at the end of mitosis undergo maturation, which drives the dynamics of PNBs up to their disappearance in G1 phase.

Discussion

The data presented here strongly converge to show that mitotic pre-rRNAs undergo processing in PNBs. FISH detection of pre-rRNAs using a broad range of probes established that pre-rRNAs

within PNBs evolve during the course of the G1 phase, following the same order as processing in nucleoli. More precisely, the disappearance of the 5'-ETS at the telophase/G1 transition is followed by the progressive removal of ITS1 and ITS2, the latter being more persistent within PNBs. This persistency of the 60S subunit precursors in PNBs corresponds to the longer maturation time of these subunits, as compared to the 40S subunits. Consistently, it was shown in monkey CMT3 that 18S rRNA precursors disappeared from PNBs after mitosis more rapidly than 28S rRNA precursors (Dundr et al., 2000). Maturation of pre-rRNAs in PNBs was further demonstrated by loss-of-function experiments, since knockdown of ribosomal proteins or pre-ribosomal factors blocked the maturation of pre-rRNAs in PNBs. Specific pre-rRNAs accumulated in PNBs depending on the maturation stage affected by protein knockdown, together with specific nucleolar factors (pre-ribosomal proteins, snoRNAs), which indicates that these domains contain pre-ribosomal particles whose maturation was interrupted. Indeed, direct visualisation of PNBs by electron tomography revealed the presence of putative pre-ribosomes, whose size was compatible with the accumulation of pre-40S particles in RPS19-depleted cells.

In the light of the present data, PNBs emerge as autonomous extra-nucleolar sites in which processing of mitotic pre-rRNAs takes place. This description of PNBs is compatible with the dynamic nature of these structures, which allows for the rapid exchange of pre-ribosomal factors, as observed for fibrillarin,

Nop52 and B23 using FRAP and photo-activation experiments (Dundr et al., 2000; Muro et al., 2010). In addition, Nop52 and B23, which are involved in ITS2 processing, are dissociated in the mitotic chromosomal sheath, but do form a complex in PNBs, indicating that pre-ribosomal factors establish functional interactions in PNBs (Angelier et al., 2005). The presence of pre-ribosomal factors in these foci appears to follow the same pattern as in nucleoli, as shown here for the early and late factors of the 40S maturation pathway: the late factors hRio2 and hLtv1, which are not found in nucleoli, do not accumulate in PNBs either, while bystin/hEnp1, hDim2 and hNoc4 are found both in nucleoli and in PNBs. As described for nucleoli, the structure of PNBs may be maintained through self-organisation of the processing complexes around pre-rRNAs. This interpretation of PNB structure is supported by recent data that showed that several types of coding or non-coding RNAs can nucleate the formation of nuclear bodies (Mao et al., 2011; Shevtsov and Dundr, 2011). However, unlike nucleoli, the position of PNBs in the nucleus is not constrained by rDNA chromosomal loci (NORS). In this respect, it is possible to draw a parallel between PNBs and the small autonomous nucleolar domains (mini-nucleoli) that form when ribosomal genes are spread on individual plasmids in *S. cerevisiae* (Oakes et al., 1998; Trumtel et al., 2000).

In reforming nucleoli, recruitment of the nucleolar components follows the order of pre-rRNA maturation and is presumably dictated by the presence of pre-rRNAs. Our data strongly argue

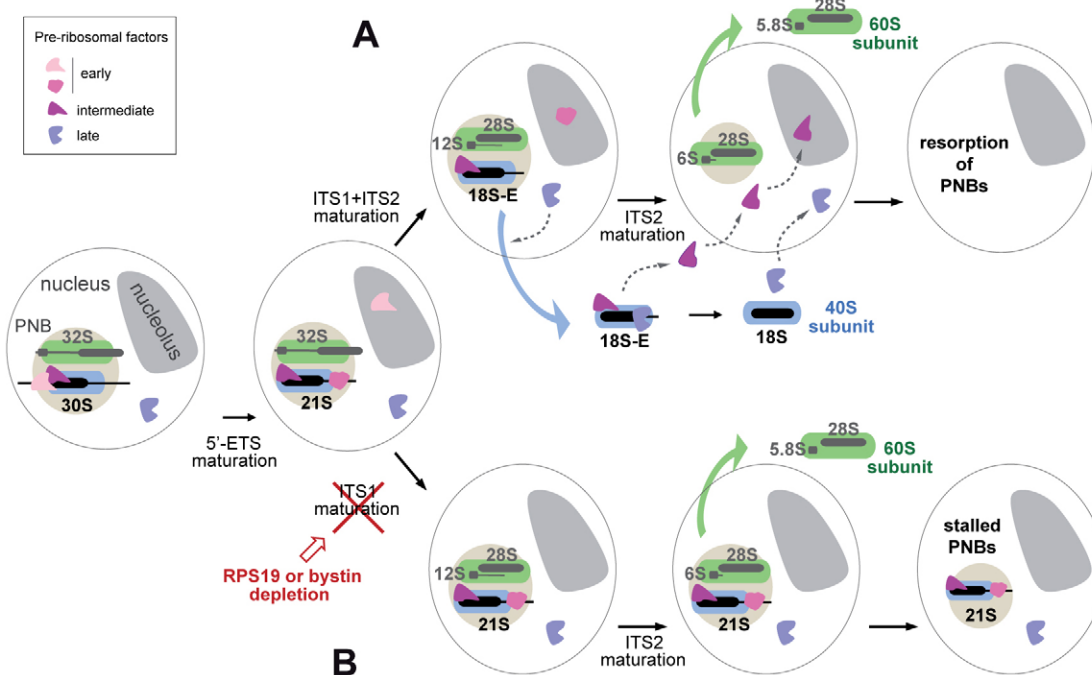


Fig. 8. A model of PNB dynamics as a pre-rRNA-processing-driven process. This model takes into account the data described in the present paper as well as previously published literature. In telophase, the mitotic pre-rRNAs and proteins of the processing machinery concentrate in PNBs where maturation is reactivated. The earliest pre-ribosomal factors are rapidly released and relocate to the incipient nucleoli. (A) In control cells, factors involved in early and intermediate processing steps are present in PNBs, where they act in pre-rRNA maturation; some progressively relocate to the nucleoli, while others remain associated to the 18S-E pre-rRNA and are joined by late pre-ribosomal factors. Pre-40S particles are exported to the cytoplasm, where the final maturation steps takes place. Late PNBs only contain pre-60S particles, the nuclear export of which leads to full disintegration of PNBs. (B) Induction of a ribosomal processing defect leads to accumulation of ill-matured pre-ribosomes in PNBs. In the case illustrated here for bystin or RPS19 depletion, pre-40S particles containing 21S pre-rRNA and 90S/pre-40S-specific factors are stalled in PNBs, which blocks dissolution of PNBs.

that, conversely, the driving force behind the disassembly of PNBs is the progressive release of pre-ribosomal factors whose role in pre-ribosome maturation has been fulfilled. In this model (Fig. 8), the release from PNBs of early acting factors takes place at the same time as the processing of the most immature pre-rRNA species at telophase (Fig. 8A). Afterwards, intermediate processing factors involved in the 40S subunit maturation pathway are released next. Some of these are exported to the cytoplasm together with pre-40S particles. Ultimately, PNBs only contain pre-60S particles, which are progressively exported from the nucleus. As predicted from this model, blocking pre-rRNA maturation is sufficient to prevent disassembly of PNBs. Hence, when RPS19 or bystin/hEnp1 are depleted (Fig. 8B), pre-60S particles are matured in PNBs and exported to the cytoplasm, but the pre-40S particles accumulate, thus blocking resorption of PNBs.

Although our current description of PNBs does not contradict previous data, it does call for a partial re-interpretation of some results. While they have mostly been envisioned as domains involved in post-mitotic reformation of nucleoli, PNBs appear to be dedicated to mitotic pre-rRNA processing, in parallel with, but independently of, the processing of neo-synthesised pre-rRNAs in the incipient nucleoli. To our knowledge, data showing a direct causal link between the dynamics of PNBs and the reformation of nucleoli at the end of mitosis are still to be established. The maintaining of assembled pre-ribosomes through mitosis is indeed likely to promote priming of the pre-rRNA processing machinery in daughter cells. In addition, several signalling pathways have now been shown to induce cell cycle arrest in interphasic cells in response to ribosome biogenesis defects (Boulon et al., 2010). One may speculate that resumption of intermediate and late steps of pre-rRNA processing immediately at the end of mitosis in PNBs, including those that fuse with incipient nucleoli, prevents untimely activation of these ribosomal stress responses during reformation of nucleoli. Noticeably, haplo-insufficiency of several ribosomal proteins, including RPS19, RPS24 and RPL5, is responsible for Diamond-Blackfan anemia, a congenital erythroblastopenia (Ellis and Gleizes, 2011), which could correspond to a physiological situation where defects in PNB dynamics occur. Finally, as autonomous pre-rRNA processing domains, PNBs could prove to be a good experimental model to analyse the formation of pre-ribosomes *in situ* and study nucleolar dysfunctions, as initiated here by imaging pre-ribosomes directly in PNBs using correlative electron tomography.

Materials and Methods

Cell culture and reagents

Human cervical carcinoma HeLa cells were cultured in Dulbecco's modified Eagle's medium (DMEM) supplemented with 10% fetal calf serum (FCS) and 1 mM sodium pyruvate, in 5% CO₂ at 37 °C. HeLa cells, stably expressing EGFP fused to the N-terminus of the nucleolar factor B23 (HeLa GFP-B23 cells) or EYFP fused to the C-terminus of RPL29 (HeLa RPL29-YFP), were kindly provided by Drs D. Hernandez-Verdun (Louvet et al., 2005) and U. Kutay (Wild et al., 2010), respectively. Transient expression of GFP-Noc4 (cloned in the HindIII-XbaI sites of pEGFP-C3), GFP-Bop1 (cloned in the EcoRI site of pEGFP-C2, a gift from Dr D. Pestov) or GFP-Nop52 (cloned in the EcoRI site of pEGFP-C2, a gift from Dr P. Roussel) was performed by electrotransformation of 1 µg plasmid/10⁶ cells, as described in the next section.

Knockdown of protein expression

Different 21-mer siRNAs were used to knock down expression of the following human proteins: for RPS5 (GenBank accession no. NM_001009), 5'-CCGAGUAUGUCAGAUCAAdTdT-3' (*rps5* siRNA); for RPS6 (GenBank accession no. NM_001010), 5'-GACGCAGACUUUCUCUdTdT-3' (*rps6* siRNA); for

RPS19 (GenBank accession no. NM_001022), 5'-AGAGCUUGCUCUCCUAC-GAAdTdT-3' (*rps19* siRNA); for RPS24 (GenBank accession no. NM_033022), 5'-CACCGGAUGUCAUCUUUGdTdT-3' (*rps24* siRNA); for RPS29 (GenBank accession no. NM_001032), 5'-CGGUCUGAUCCGGAAUUAudTdT-3' (*rps29* siRNA); for RPL5 (GenBank accession no. NM_000969), 5'-GCCACAA-UGUUGCAGAUUAudTdT-3' (*rpl5* siRNA); for Bystin (GenBank accession no. NM_004053), 5'-CUGCCAAGGGCAUUAAGAdTdT-3' (*bystin-1* siRNA) and 5'-GAGGUUGAGACAGUCAUGdTdT-3' (*bystin-2* siRNA). All siRNAs were purchased from Eurogentec and provided as duplexes diluted 100 µM. 10 µl of siRNA solution were added to 10⁷ HeLa cells in suspension in 200 µl of DMEM without FCS. For bystin knockdown, a mixture of 10 µl each of *bystin-1* and *bystin-2* siRNAs were used. For controls, cells were electro-transformed either with a scramble siRNA or without siRNA, which lead to similar results. Electroporation was performed at 250 V and 970 µF with a Gene Pulser (Bio-Rad Laboratories), in a cuvette with a 4-mm inter-electrode distance. The cells were diluted in 20 ml DMEM supplemented with FCS and antibiotics and plated in a 140-cm² Petri dish for RNA extraction and northern blot analyses. They were also seeded either on glass coverslips laid in 24-well microplates for FISH and immunofluorescence assays, or on glass-bottomed Petri dishes 35 mm in diameter (Dominique Dutscher) for live-cell imaging.

Northern blot analysis of pre-rRNA

Total RNAs were purified with Trizol reagent. After alcohol precipitation, RNA pellets were dissolved in formamide, quantified using a Nanodrop spectrophotometer (Thermo Fisher Scientific) and diluted to 1 mg/ml. Pre-rRNA analysis by northern blot was performed as described previously (O'Donohue et al., 2010) with the following probes: 18S (5'-TTTACTTCCTCTAGATAGTCAAGT-TCGACC-3'), 28S (5'-CCGTTCCCTGGCTGTGTTTCGCTAGATA-3'), 5'-ITS1 (5'-CCTCGCCCTCCGGCTCCGTTAATGATC-3'), ITS2-b (5'-CTGC-GAGGAAACCCCCAGCCGC-3'), and ITS2-d/e (5'-GCGCGACGGCG-GACGACACCGCGCGTC-3'). For detection of the ITS2, the ITS2-b and ITS2-d/e probes were mixed in equal amounts. After hybridisation, the membranes were washed twice for 10 min in 2× SSC, SDS 0.1%, and once in 1× SSC, SDS 0.1%. Labelled RNA signals were acquired with a phosphorimager (FLA2000; Fuji) and quantified with the Image Gauge software.

Labelling of cellular DNA with EdU

Cells were incubated with 20 µM 5-ethynyl-2'-deoxyuridine (EdU, Invitrogen), an analogue of thymidine (Salic and Mitchison, 2008), in culture medium for 4 h. At the end of the reaction time (which corresponded to 48 h post-transfection), the cells were rinsed twice in PBS and fixed with 4% paraformaldehyde in PBS for 15 min. After several washes in PBS, cells were permeabilised for 5 min in 0.5% Triton X-100 diluted in PBS. They were then rinsed twice in PBS containing 3% BSA. EdU incorporated into DNA was revealed by click chemistry through the reaction of its terminal alkyne group with an azide derivative coupled to Alexa-594 (Invitrogen). The reaction was developed for 30 min in the presence of TBS buffer (150 mM NaCl, 50 mM Tris-HCl, pH 8.0) containing 4 mM CuSO₄, 10 µM Alexa-594 azide, 2 mg/ml ascorbic acid. The coverslips were protected from light and incubated at ambient temperature under slow agitation. The cells were then rinsed briefly in TBS buffer. PNBs were revealed by FISH with the 5'ITS1 probe conjugated to Alexa-488 (O'Donohue et al., 2010). After two washes in 2× SSC containing 10% formamide, DNA was counter-stained with Hoechst 33342 (Invitrogen) and the coverslips were mounted in Mowiol (version 4.88; PolyScience, Inc.).

Fluorescence *in situ* hybridisation and immunofluorescence assays

Pre-rRNA species were localised by fluorescence *in situ* hybridisation (FISH) as described (O'Donohue et al., 2010). Appropriate combinations of the following probes, conjugated to Cy3, Cy5 or Alexa-488, were chosen in order to reveal various subsets of pre-rRNA species: ETS1-297 (5'-AGACGAGAACGCCTGACACGACGGC-3'), ETS1-1399 (5'-CGCTAGAGAACGGCTTC-3'), 5'ITS1 (5'-GATCAAACCGAGTAGGTAAAGGTAGAGCGGGCGA-3'), 5'ITS1 (5'-CCTCGCCCTCCGGGCTCCGTTAATGATC-3'), ITS1-160 (5'-TCTC-CCTCCGAGTCTCGGCTCT-3'), 5.8S-ITS2 (5'-GCGATTGATCGGAAG-CGACGCTC-3'), 28S-ETS2 (5'-CGTGCCTGCGCGCCCTGTTGGGA-AC-3'). For snoRNAs, probes rU3 (5'-TTGCACAGAACGACCTAGAG-CGGCTTCACGCTT-3') and hU8 (5'-ATAGGAGCAATCAGGATGTTGCAA-GACCTGATTACGCAAGAGCGTT-3') conjugated in their 5' end to Cy3 were used. Cells grown on glass coverslips were fixed with 4% paraformaldehyde in PBS for 30 min. After washing in PBS, the cells were permeabilised in 70% ethanol overnight at 4°C. They were then rehydrated twice for 5 min in 2× SSC containing 10% formamide. Hybridisations in the presence of two to three different probes and further processing of the coverslips were as described in the previous section.

For immunofluorescence studies, cells grown on glass coverslips were fixed for 15 min with 4% paraformaldehyde in PBS. After washing in PBS, cells were permeabilised for 5 min in 0.1% Triton X-100 and 0.02% SDS in PBS. Saturation was performed for 30 min first in 2% BSA in PBS, and then in 10% normal goat serum (NGS) in PBS. The primary antibody, diluted in 10% NGS in PBS, was put

in contact with the cells for 1 h at room temperature. The antisera were: anti-Rio2 (1:5000), anti-Nob1 (1:5000), anti-Dim2 (1:2000) [all gifts from Dr U. Kutay (Zemp et al., 2009)], [anti-bystin (1:10,000), anti-Ltv1 (1:20,000); both raised in our laboratory], and anti-fibrillarin (1:1000; a gift from Dr J. Cavaillé). After washing in 2% BSA in PBS, and in 10% NGS in PBS, cells were incubated with the secondary antibody coupled to Alexa-488, 555 or 647 and diluted 1:4000 in 10% NGS in PBS. After washing briefly in 0.1% Triton X-100 and 0.02% SDS in PBS, DNA counterstaining with Hoechst and mounting were as described above.

Light microscopy observations and time-lapse experiments

Observations of fixed cells were made with an inverted microscope (IX-81; Olympus), equipped with a motorized stage (Märzhäuser) and a camera (Coolsnap HQ; Photometrics), driven by MetaMorph (MDS Analytical Technologies). Cells were observed using a $\times 100$, oil immersion objective (Plan Apochromat, 1.4 NA; Olympus) driven by a piezo z-stepper (PI). The pixel size was 64.5 nm. The light source was a monochromator (Polychrome V; Till Photonics GmbH) equipped with a 150 W Xenon source and used with a 15-nm bandwidth. For multi-labelling experiments, multiband dichroic mirrors (Chroma) were used to avoid pixel shift in the acquisition plane. Specific single-band emission filters were mounted on a motorized wheel (PI). To analyse Edu incorporation experiments by image cytometry, adjacent fields were systematically acquired in each experimental condition, until an appropriate number of cells had been reached (between 700 and 1100 cells). By using Hoechst and 5'ITS1 labelling, each nucleus was then checked for its content in PNBS. In each group, EdU-labelled versus unlabelled cells were assessed.

Time-lapse experiments were done at 37°C on live HeLa GFP-B23 cells 48 h post-transfection with siRNAs. Images were acquired with the wide-field microscope described above with a 0.3 μm z-step. Alternatively, 3D time-lapse experiments were performed with an Andor Revolution Nipkow-disk confocal system installed on an inverted microscope (IX-81; Olympus), featuring a confocal spinning disk unit (CSU22; Yokogawa) and a cooled EM-CCD camera (Andor). For illumination, the 488-nm line of a diode pumped solid-state laser (25 mW; Coherent) was used at 30% of its power. With a 100 \times oil immersion objective (Plan Apochromat, 1.4 NA; Olympus), the pixel size was 77 nm. The exposure was set to 100 ms per plane. For comparison purposes, cells in anaphase or very early telophase were selected, as the former is the shortest step of mitosis. Images were captured every 3 min over 2 h in order to follow the last steps of mitosis and early G1. Alternatively, they were acquired every 10 min for the first 3 h, and then every 30 min for up to 8 h in order to study the behaviour of residual PNBS during G1 phase in siRNA-treated cells. Deconvolution, maximum intensity projections and image analyses were performed with MetaMorph software (Molecular Devices).

Correlative electron tomography

HeLa GFP-B23 cells were prepared for TEM by overnight fixation at 4°C with 3% paraformaldehyde and 0.1% glutaraldehyde in phosphate buffer (pH 7.2). They were collected by scrapping, centrifuged briefly and the pellet was included in agarose. Embedding in resin was performed according to the Progressive Lowering of Temperature method using an automatic freeze-substitution system (EM AFS2; Leica Microsystems). The cells were cryoprotected with 3.5% sucrose and stained with 1% uranyl acetate. After dehydrating with ethanol while decreasing the temperature from 0°C to -30°C, the samples were infiltrated with Lowicryl HM20 resin which was polymerized under UV light for 2 days at -30°C. To perform correlative microscopy, ultra-thin sections were cut on a UC6 ultramicrotome (Leica Microsystems) at room temperature with a nominal thickness of 150 nm using an ultra 45° diamond knife (Diatome Inc.) and deposited on formvar-carbon-coated Finder grids (EMS). The grids were mounted on a glass slide in 50% glycerol and observed by fluorescence microscopy to detect PNBS with GFP-B23. The alphanumerical code of the Finder grids was used to position the cells of interest. The grids were then removed from the glass slides, extensively washed in water to remove glycerol, stained with uranyl acetate and lead citrate and 10 nm-diameter colloidal gold particles were deposited onto both sides. Electron tomography was performed on the same sections by recording tilt-series at 200 kV with a LaB₆ TEM (JEM-2100; Jeol) equipped with a 2 \times 2 k US1000 CCD camera and driven by Digital Micrograph software (Gatan Inc.). The angular range was -60° to 60° sampled with 2° increments. The nominal magnification was 15,000 \times , which resulted in a pixel size of 6.9 Å at the specimen level. Tomographic reconstructions were performed with the simultaneous iterative reconstruction technique provided by IMOD software (Kremer et al., 1996) using the 10 nm gold particles as fiducial markers for aligning the image stack. Particles were visualised with the University of California San Francisco Chimera package (Petersen et al., 2004) using the Segment Map function from the Segger package (Pintilie et al., 2010). For measurement of their size, particles were manually extracted from the reconstructed tomograms and a bounding box was adjusted around the middle section of each particle. The longest and shortest dimensions were attributed to the length and width, respectively. These bounding boxes were compared with those obtained from the X-ray crystal structures of the yeast 40S and 60S ribosomal subunits [Protein Data Bank accessing codes 3O2Z and 3O58,

respectively (Ben-Shem et al., 2010)]. In order to do so, the structures were filtered at 80 Å resolution and converted to mrc format with a 6.9 Å per pixel step, using Chimera. Projections of the filtered 3D models were then computed using IMAGIC-5 (van Heel et al., 1996). For each 3D model, a set of 108 projections uniformly distributed within the asymmetric triangle was produced, using an angular increment of 20° along the longitudinal axis. The projections were then normalised and binarised with a 1σ threshold and the dimensions of the bounding boxes fitting the projection were measured with IMOD as described above. Electron tomography was performed at the electron microscopy facility of the Fédération de Recherche en Biologie de Toulouse.

Acknowledgements

The authors are grateful to Drs Ulrike Kutay for the gift of antisera and of the HeLa RPL29-YFP cell line; Danièle Hernandez-Verdun and Pascal Roussel for the HeLa GFP-B23 cell line and the pEGFP-Nop52 construct; Dimitri Pestov for pEGFP-Bop1; Céline Verheggen and Jérôme Cavaillé for snoRNA probes; and Christophe Normand for his help with the spinning disk confocal microscope. The authors also wish to thank Dr C. Verheggen for her early interest in this study and helpful advice, Valérie Choesmel for her involvement at the beginning of the project and Drs Jérôme Cavaillé, François Morlé and Boris Guyot for scientific discussions. Pierre-Emmanuel Gleizes and Marie-Françoise O'Donohue contributed equally to this work as senior authors.

Funding

This project was funded by the Centre National de la Recherche Scientifique (CNRS); the University of Toulouse, the French National Research Agency [grant number ANR-06-BLAN-0037 to P.E.G.]; the Association pour la Recherche contre le Cancer [grant number 1058 to P.E.G.]; and the Institut Universitaire de France to P.E.G. C.C. was supported by fellowships from the Ministère de l'Éducation Nationale et de la Recherche and the Association pour la Recherche sur le Cancer.

Supplementary material available online at
<http://jcs.biologists.org/lookup/suppl/doi:10.1242/jcs.106419/-DC1>

References

- Angelier, N., Tramier, M., Louvet, E., Coppey-Moisan, M., Savino, T. M., De Mey, J. R. and Hernandez-Verdun, D. (2005). Tracking the interactions of rRNA processing proteins during nucleolar assembly in living cells. *Mol. Biol. Cell* **16**, 2862-2871.
- Azum-Gélade, M. C., Noaillac-Depeyre, J., Caizergues-Ferrer, M. and Gas, N. (1994). Cell cycle redistribution of U3 snRNA and fibrillarin. Presence in the cytoplasmic nucleolus remnant and in the prenucleolar bodies at telophase. *J. Cell Sci.* **107**, 463-475.
- Ben-Shem, A., Jenner, L., Yusupova, G. and Yusupov, M. (2010). Crystal structure of the eukaryotic ribosome. *Science* **330**, 1203-1209.
- Beven, A. F., Lee, R., Razaz, M., Leader, D. J., Brown, J. W. and Shaw, P. J. (1996). The organization of ribosomal RNA processing correlates with the distribution of nucleolar snRNAs. *J. Cell Sci.* **109**, 1241-1251.
- Borovjagin, A. V. and Gerbi, S. A. (2005). An evolutionary intra-molecular shift in the preferred U3 snoRNA binding site on pre-ribosomal RNA. *Nucleic Acids Res.* **33**, 4995-5005.
- Boulon, S., Westman, B. J., Hutten, S., Boisvert, F. M. and Lamond, A. I. (2010). The nucleolus under stress. *Mol. Cell* **40**, 216-227.
- Chan, E. K., Imai, H., Hamel, J. C. and Tan, E. M. (1991). Human autoantibody to RNA polymerase I transcription factor hUBF. Molecular identity of nucleolus organizer region autoantigen NOR-90 and ribosomal RNA transcription upstream binding factor. *J. Exp. Med.* **174**, 1239-1244.
- Chen, D., Dundr, M., Wang, C., Leung, A., Lamond, A., Misteli, T. and Huang, S. (2004). Condensed mitotic chromatin is accessible to transcription factors and chromatin structural proteins. *J. Cell Biol.* **168**, 41-54.
- DiMario, P. J. (2004). Cell and molecular biology of nucleolar assembly and disassembly. *Int. Rev. Cytol.* **239**, 99-178.
- Dousset, T., Wang, C., Verheggen, C., Chen, D., Hernandez-Verdun, D. and Huang, S. (2000). Initiation of nucleolar assembly is independent of RNA polymerase I transcription. *Mol. Biol. Cell* **11**, 2705-2717.
- Dundr, M. and Olson, M. O. (1998). Partially processed pre-rRNA is preserved in association with processing components in nucleolus-derived foci during mitosis. *Mol. Biol. Cell* **9**, 2407-2422.
- Dundr, M., Misteli, T. and Olson, M. O. (2000). The dynamics of postmitotic reassembly of the nucleolus. *J. Cell Biol.* **150**, 433-446.

- Eichler, D. C. and Craig, N.** (1994). Processing of eukaryotic ribosomal RNA. *Prog. Nucleic Acid Res. Mol. Biol.* **49**, 197-239.
- Ellis, S. R. and Gleizes, P. E.** (2011). Diamond Blackfan anemia: ribosomal proteins going rogue. *Semin. Hematol.* **48**, 89-96.
- Fan, H. and Penman, S.** (1971). Regulation of synthesis and processing of nucleolar components in metaphase-arrested cells. *J. Mol. Biol.* **59**, 27-42.
- Fatica, A. and Tollervey, D.** (2002). Making ribosomes. *Curr. Opin. Cell Biol.* **14**, 313-318.
- Fomproix, N. and Hernandez-Verdun, D.** (1999). Effects of anti-PM-Scl 100 (Rrp6p exonuclease) antibodies on prenucleolar body dynamics at the end of mitosis. *Exp. Cell Res.* **251**, 452-464.
- Gébrane-Younès, J., Fomproix, N. and Hernandez-Verdun, D.** (1997). When rDNA transcription is arrested during mitosis, UBF is still associated with non-condensed rDNA. *J. Cell Sci.* **110**, 2429-2440.
- Hadjiolov, A. A.** (1985). The nucleolus and ribosome biogenesis. In *Cell Biology Monographs*, Vol. 12 (ed. M. Alfert, W. Beermann, L. Goldstein, K. R. Porter and P. Sitte), 268 pp. Wien, Austria: Springer-Verlag.
- Heix, J., Vente, A., Voit, R., Budde, A., Michaelidis, T. M. and Grummt, I.** (1998). Mitotic silencing of human rRNA synthesis: inactivation of the promoter selectivity factor SL1 by cdc2/cyclin B-mediated phosphorylation. *EMBO J.* **17**, 7373-7381.
- Henras, A. K., Soudet, J., Gérus, M., Lebaron, S., Caizergues-Ferrer, M., Mougin, A. and Henry, Y.** (2008). The post-transcriptional steps of eukaryotic ribosome biogenesis. *Cell. Mol. Life Sci.* **65**, 2334-2359.
- Jiménez-García, L. F., Segura-Valdez, M. L., Ochs, R. L., Rothblum, L. I., Hannan, R. and Spector, D. L.** (1994). Nucleologenesis: U3 snRNA-containing prenucleolar bodies move to sites of active pre-rRNA transcription after mitosis. *Mol. Biol. Cell* **5**, 955-966.
- Kremer, J. R., Mastronarde, D. N. and McIntosh, J. R.** (1996). Computer visualization of three-dimensional image data using IMOD. *J. Struct. Biol.* **116**, 71-76.
- Kressler, D., Hurt, E. and Bassler, J.** (2010). Driving ribosome assembly. *Biochim. Biophys. Acta* **1803**, 673-683.
- Lamanna, A. C. and Karbstein, K.** (2009). Nob1 binds the single-stranded cleavage site D at the 3'-end of 18S rRNA with its PIN domain. *Proc. Natl. Acad. Sci. USA* **106**, 14259-14264.
- Lapik, Y. R., Fernandes, C. J., Lau, L. F. and Pestov, D. G.** (2004). Physical and functional interaction between Pes1 and Bop1 in mammalian ribosome biogenesis. *Mol. Cell* **15**, 17-29.
- Leung, A. K., Gerlich, D., Miller, G., Lyon, C., Lam, Y. W., Lleres, D., Daigle, N., Zomerdiijk, J., Ellenberg, J. and Lamond, A. I.** (2004). Quantitative kinetic analysis of nucleolar breakdown and reassembly during mitosis in live human cells. *J. Cell Biol.* **166**, 787-800.
- Lindström, M. S.** (2011). NPM1/B23: A multifunctional chaperone in ribosome biogenesis and chromatin remodeling. *Biochem. Res. Int.* **2011**, doi:10.1155/2011/195209.
- Louvet, E., Junéra, H. R., Le Panse, S. and Hernandez-Verdun, D.** (2005). Dynamics and compartmentation of the nucleolar processing machinery. *Exp. Cell Res.* **304**, 457-470.
- Mao, Y. S., Sunwoo, H., Zhang, B. and Spector, D. L.** (2011). Direct visualization of the co-transcriptional assembly of a nuclear body by noncoding RNAs. *Nat. Cell Biol.* **13**, 95-101.
- Miyake, K., Utsugisawa, T., Flygare, J., Kiefer, T., Hamaguchi, I., Richter, J. and Karlsson, S.** (2008). Ribosomal protein S19 deficiency leads to reduced proliferation and increased apoptosis but does not affect terminal erythroid differentiation in a cell line model of Diamond-Blackfan anemia. *Stem Cells* **26**, 323-329.
- Muro, E., Gébrane-Younis, J., Jobart-Malfait, A., Louvet, E., Roussel, P. and Hernandez-Verdun, D.** (2010). The traffic of proteins between nucleolar organizer regions and prenucleolar bodies governs the assembly of the nucleolus at exit of mitosis. *Nucleus* **1**, 202-211.
- O'Donohue, M. F., Choesmel, V., Faubladier, M., Fichant, G. and Gleizes, P. E.** (2010). Functional dichotomy of ribosomal proteins during the synthesis of mammalian 40S ribosomal subunits. *J. Cell Biol.* **190**, 853-866.
- Oakes, M., Aris, J. P., Brockenbrough, J. S., Wai, H., Vu, L. and Nomura, M.** (1998). Mutational analysis of the structure and localization of the nucleolus in the yeast *Saccharomyces cerevisiae*. *J. Cell Biol.* **143**, 23-34.
- Pérez-Fernández, J., Román, A., De Las Rivas, J., Bustelo, X. R. and Dosil, M.** (2007). The 90S preribosome is a multimodular structure that is assembled through a hierarchical mechanism. *Mol. Cell. Biol.* **27**, 5414-5429.
- Pettersen, E. F., Goddard, T. D., Huang, C. C., Couch, G. S., Greenblatt, D. M., Meng, E. C. and Ferrin, T. E.** (2004). UCSF Chimera—a visualization system for exploratory research and analysis. *J. Comput. Chem.* **25**, 1605-1612.
- Piñol-Roma, S.** (1999). Association of nonribosomal nucleolar proteins in ribonucleoprotein complexes during interphase and mitosis. *Mol. Biol. Cell* **10**, 77-90.
- Pintilie, G. D., Zhang, J., Goddard, T. D., Chiu, W. and Gossard, D. C.** (2010). Quantitative analysis of cryo-EM density map segmentation by watershed and scale-space filtering, and fitting of structures by alignment to regions. *J. Struct. Biol.* **170**, 427-438.
- Rouquette, J., Choesmel, V. and Gleizes, P. E.** (2005). Nuclear export and cytoplasmic processing of precursors to the 40S ribosomal subunits in mammalian cells. *EMBO J.* **24**, 2862-2872.
- Roussel, P., André, C., Masson, C., Géraud, G. and Hernandez-Verdun, D.** (1993). Localization of the RNA polymerase I transcription factor hUBF during the cell cycle. *J. Cell Sci.* **104**, 327-337.
- Roussel, P., André, C., Comai, L. and Hernandez-Verdun, D.** (1996). The rDNA transcription machinery is assembled during mitosis in active NORs and absent in inactive NORs. *J. Cell Biol.* **133**, 235-246.
- Salic, A. and Mitchison, T. J.** (2008). A chemical method for fast and sensitive detection of DNA synthesis in vivo. *Proc. Natl. Acad. Sci. USA* **105**, 2415-2420.
- Savino, T. M., Bastos, R., Jansen, E. and Hernandez-Verdun, D.** (1999). The nucleolar antigen Nop52, the human homologue of the yeast ribosomal RNA processing RRP1, is recruited at late stages of nucleologenesis. *J. Cell Sci.* **112**, 1889-1900.
- Savino, T. M., Gébrane-Younès, J., De Mey, J., Sibarita, J. B. and Hernandez-Verdun, D.** (2001). Nucleolar assembly of the rRNA processing machinery in living cells. *J. Cell Biol.* **153**, 1097-1110.
- Shevtsov, S. P. and Dundr, M.** (2011). Nucleation of nuclear bodies by RNA. *Nat. Cell Biol.* **13**, 167-173.
- Sirri, V., Roussel, P. and Hernandez-Verdun, D.** (1999). The mitotically phosphorylated form of the transcription termination factor TTF-1 is associated with the repressed rDNA transcription machinery. *J. Cell Sci.* **112**, 3259-3268.
- Srivastava, L., Lapik, Y. R., Wang, M. and Pestov, D. G.** (2010). Mammalian DEAD box protein Ddx51 acts in 3' end maturation of 28S rRNA by promoting the release of U8 snoRNA. *Mol. Cell. Biol.* **30**, 2947-2956.
- Thomson, E. and Tollervey, D.** (2010). The final step in 5.8S rRNA processing is cytoplasmic in *Saccharomyces cerevisiae*. *Mol. Cell. Biol.* **30**, 976-984.
- Trumtel, S., Léger-Silvestre, I., Gleizes, P. E., Teulières, F. and Gas, N.** (2000). Assembly and functional organization of the nucleolus: ultrastructural analysis of *Saccharomyces cerevisiae* mutants. *Mol. Biol. Cell* **11**, 2175-2189.
- van Heel, M., Harauz, G., Orlova, E. V., Schmidt, R. and Schatz, M.** (1996). A new generation of the IMAGIC image processing system. *J. Struct. Biol.* **116**, 17-24.
- Wild, T., Horvath, P., Wyler, E., Widmann, B., Badertscher, L., Zemp, I., Kozak, K., Csucs, G., Lund, E. and Kutay, U.** (2010). A protein inventory of human ribosome biogenesis reveals an essential function of exportin 5 in 60S subunit export. *PLoS Biol.* **8**, e1000522.
- Zatsypina, O. V., Voit, R., Grummt, I., Spring, H., Semenov, M. V. and Trendelenburg, M. F.** (1993). The RNA polymerase I-specific transcription initiation factor UBF is associated with transcriptionally active and inactive ribosomal genes. *Chromosoma* **102**, 599-611.
- Zemp, I., Wild, T., O'Donohue, M. F., Wandrey, F., Widmann, B., Gleizes, P. E. and Kutay, U.** (2009). Distinct cytoplasmic maturation steps of 40S ribosomal subunit precursors require hRIO2. *J. Cell Biol.* **185**, 1167-1180.